

# Diffusion Tensor Imaging of Microstructural Changes in the Gray and White Matter in Patients With Crigler-Najjar Syndrome Type I

Ahmed Abdel Khalek Abdel Razek, MD,\* Saher Ebrahiem Taman, MD,\* Mohamed Ezz El Regal, MD,†  
Ahmed Megahed, MD,‡ Sherine Elzeny, MD,‡ and Noha El Tantawi, MD‡

**Purpose:** This study aimed to evaluate the role of diffusion tensor imaging of microstructural changes in gray and white matter in Crigler-Najjar syndrome type I.

**Patient and Methods:** A prospective study was conducted on 10 patients with Crigler-Najjar syndrome type I and 10 age- and sex-matched children who underwent diffusion tensor imaging of the brain. Mean diffusivity (MD) and fractional anisotropy (FA) of gray and white matter were measured.

**Results:** There was a significantly higher MD of the gray matter regions including the globus pallidus, thalamus, caudate head, substantia nigra, and dentate nucleus in patients versus controls ( $P = 0.007, 0.001, 0.014, 0.003,$  and  $0.002$ ), respectively. The areas under the curve (AUC) of MD of the globus pallidus and thalamus used to differentiate patients from controls were 0.93 and 0.925, respectively. There was a significant difference in MD of the frontal white matter and posterior limb of the internal capsule in patients versus controls ( $P = 0.001$  and  $0.02$ ), respectively. The AUCs of MD of these regions used to differentiate patients from controls were 0.82 and 0.8. There was a significant difference in FA of the frontal white matter and posterior limb of the internal capsule in patients versus controls ( $P = 0.006$  and  $0.006$ ), respectively. The AUCs of FA of these regions were 0.83 and 0.85, respectively. The MD of the globus pallidus correlated with serum bilirubin ( $r = 0.87$  and  $P = 0.001$ ).

**Conclusion:** Diffusion tensor imaging can detect microstructural changes of deep gray matter and some regions of white matter in Crigler-Najjar syndrome type I.

**Key Words:** diffusion tensor, Crigler-Najjar, brain, imaging

(*J Comput Assist Tomogr* 2020;00: 00–00)

Crigler-Najjar syndrome is a very rare familial, genetic inborn error of metabolism with an incidence of 0.6 to 1.0 per million that present shortly after birth with unconjugated hyperbilirubinemia and bilirubin encephalopathy. This syndrome characterized by absent or nearly absent uridine diphosphate glucuronosyl transferase (*UGT1A1*) enzyme activity. It is manifested shortly after birth with high serum unconjugated bilirubin levels greater than 20 to 50 mg/dL. Consequently, it is associated with bilirubin encephalopathy and death unless managed by aggressive therapy in the immediate newborn period. There are 2 types of this syndrome: type I with no enzyme function and type II with less than 20% of normal enzyme function.<sup>1–5</sup> Bilirubin encephalopathy in patients with syndrome type I can occur at any age, especially during infectious episodes, fasting, or stress. The damage to the brain is not always

reversible. The most common clinical presentations are severe neurological motor and hearing impairment, which may progress to cerebral palsy. Phototherapy, orthotopic liver transplantation, liver cell transplantation, and gene therapy are treatment choices used.<sup>4–8</sup>

Magnetic resonance imaging (MRI) may show high signal intensity on T2-weighted images of the deep gray matter regions in the subacute and chronic phases.<sup>9–12</sup> These abnormal signals vary by time, so there is a need to establish additional biomarkers to help MRI to be pathognomonic and to predict chronic bilirubin encephalopathy.<sup>12,13</sup> In neonates with acute bilirubin encephalopathy, there is restricted diffusion of the globus pallidus. In the subacute and chronic phases, there is an increase in diffusivity. In infants with bilirubin encephalopathy, magnetic resonance (MR) spectroscopy demonstrated a decrease in the ratio of *N*-acetyl-aspartate (NAA) to choline and NAA to creatine as well as an increase in the ratio of lactate to NAA in the basal ganglia.<sup>11–16</sup>

Diffusion tensor imaging (DTI) can detect tissue microstructure changes that occur with different pathologies. It is also useful in the detection of long-term changes along specific anatomical pathways. The commonly used parameters are fractional anisotropy (FA) and mean diffusivity (MD).<sup>17–20</sup> It can be used to measure anisotropy per voxel. The recent development of DTI provides an indirect way of examining tissues through the isotropic/anisotropic behavior of water diffusion in the brain and has become a useful tool for investigation of different brain disorders such as epilepsy, tumors, and demyelinating disorders.<sup>21–25</sup> Few articles discuss the role of diffusion-weighted MRI in neonatal bilirubin encephalopathy.<sup>26–28</sup> To our knowledge, there is no previous English literature that discusses DTI in patients with Crigler-Najjar syndrome type I.

The aim of the study was to evaluate the role of DTI of microstructural changes in the gray and white matter in patients with Crigler-Najjar syndrome type I.

## PATIENTS AND METHODS

### Patients

The institutional ethics review and informed consents from guardians of infants and controls enrolled in this study were obtained. This prospective study included 10 infants with Crigler-Najjar syndrome type I and 10 age- and sex-matched controls who underwent MR examination for causes other than neurological disease in the period from July 2017 to May 2018. Conventional MRI with DTI of the brain was done for all patients and controls. The inclusion criteria were patients with Crigler-Najjar syndrome type I with unconjugated hyperbilirubinemia proved by laboratory results (serum bilirubin levels >20 mg/dL). The patient group included 4 boys and 6 girls, with a mean age of  $7.17 \pm 4.9$  years, and the control group was composed of 5 boys and 5 girls, with a mean age of  $6.19 \pm 4.13$  years. Follow-up serum

From the \*Department of Diagnostic Radiology, †Gastroenterology and Hepatology Unit of Mansoura Children Hospital, and ‡Neurology Unit of Mansoura Children Hospital, Mansoura Faculty of Medicine, Mansoura, Egypt. Received for publication September 1, 2019; accepted January 11, 2020.

Correspondence to: Ahmed Abdel Khalek Abdel Razek, MD, Department of Diagnostic Radiology, Mansoura Faculty of Medicine, Mansoura 13551, Egypt (e-mail: arazek@mans.edu.eg).

The authors declare no conflict of interest.

Copyright © 2020 Wolters Kluwer Health, Inc. All rights reserved.

DOI: 10.1097/RCT.0000000000001008

bilirubin level was done for all patients with recording of the highest level.

### Clinical Examination

Each patient was assessed clinically with a pediatric neurologist (E.N.) with 10 years of experience. The assessment was done for extrapyramidal symptoms and minor signs as neuromuscular incoordination, abnormalities of muscle tone, and reflexes and motor power according to Touwen's<sup>29</sup> infant neurological examination and Touwen's test modified by Hadders-Algra et al.<sup>30</sup>

### MR Imaging

All patients and controls underwent MR examination of the brain. Sedation was done using oral chloral hydrate (70–80 mg/kg body weight) 30 minutes before MR examination in 4 patients and 5 controls, and the remaining (6 patients and 5 controls) underwent examination without sedation. The MRI was done using a 1.5-T scanner (Ingenia; Philips, Philips Medical Systems, Best, the Netherlands) using a head neck 20-channel coil. First, routine sequences were performed: T1-weighted (repetition time/echo time [TR/TE], 620/20 milliseconds), T2-weighted image (TR/TE, 5430/95 milliseconds), and FLAIR (TR/TE/inversion time, 10,500/120/2800 milliseconds) with matrix of 80 × 80, field of view of 240 × 220 mm, and slice thickness of 5 mm. The DTI was

done using a single-shot echo-planar imaging sequence (TR/TE, 3118/93 milliseconds) with SENSitivity Encoding. Then diffusion gradients were applied along 32 axes using *b* values of 0 and 1000 s/mm<sup>2</sup>. A field of view of 240 × 220 mm<sup>2</sup> and data matrix of 92 × 88 were used, leading to voxel dimensions (2.43 × 2.54 × 2.5 mm). Forty-eight slices were obtained, with a thickness of 2.5 mm, no gap, and the total scan time of 7 to 8 minutes.

### Image Analysis

The image analysis was done by a pediatric neuroradiologist (T.S.) with 18 years of experience who was blinded to the clinical and laboratory data. The images were transferred to a workstation (extended MR Workspace 2.6.3.5; Philips Medical Systems, Nederland BV). A single-pixel seed isotropic region of interest was placed in 5 gray matter regions (globus pallidus, caudate head, thalamus, substantia nigra of the midbrain, and dentate nucleus of the cerebellum) and 5 white matter regions (frontal, occipital, parietal, temporal regions, and posterior limbs of the internal capsules) on both sides (Fig. 1).

### Statistical Analysis

Statistical analyses were done using Statistical Package for Social Sciences (SPSS, Chicago, Illinois), version 22. Quantitative

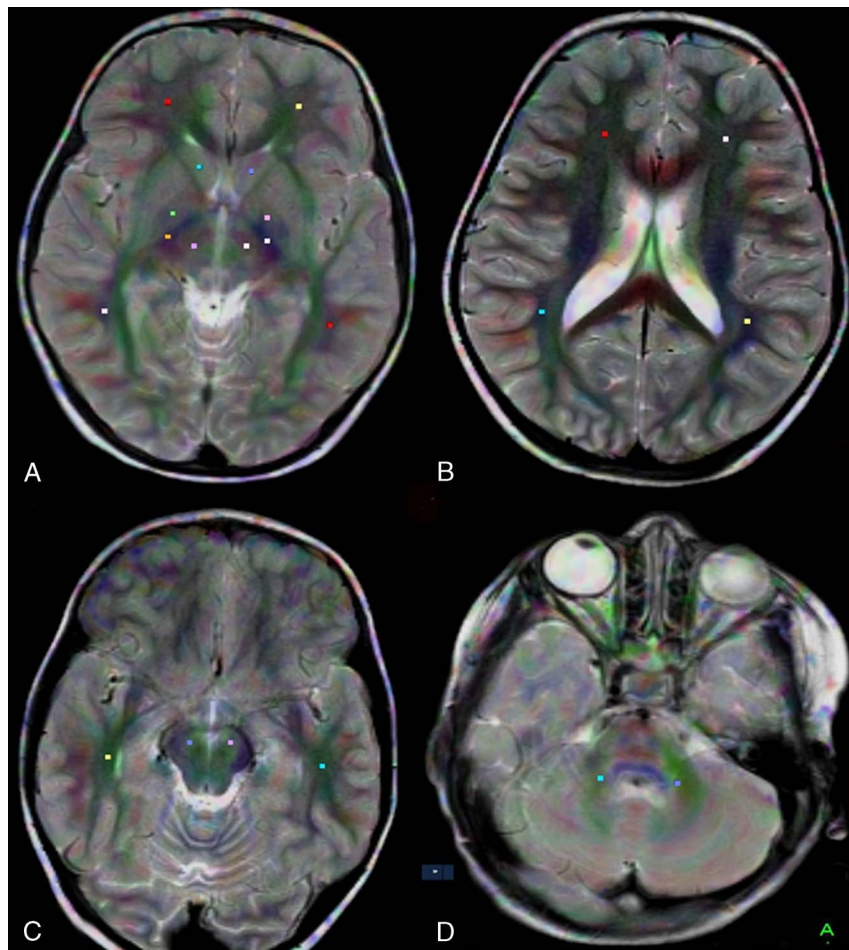


**FIGURE 1.** Regions of interest localization at different regions of the brain. A, Caudate head, thalamus, globus pallidus, posterior limb of the internal capsule, and parietal white matter. B, Frontal, parietal, and temporal white matter. C, Substantia nigra and temporal white matter. D, Cerebellar dentate nucleus.

**TABLE 1.** Demographic and Phenotyping of Patients With Crigler-Najjar Syndrome

Demographic			Phenotyping				
No	Age, y	Sex	Tone Abn.	Reflexes Abn.	Incoordination Abn.	Executive Abn.	Decreased Motor Power of UL
1	6	F	-ve	+ve	+ve	-ve	+ve
2	9.8	F	-ve	+ve	+ve	-ve	+ve
3	9	F	+ve	-ve	+ve	+ve	+ve
4	11.5	M	+ve	+ve	+ve	-ve	+ve
5	3.5	M	+ve	+ve	+ve	+ve	+ve
6	1.7	F	+ve	+ve	-ve	+ve	-ve
7	14	F	+ve	+ve	-ve	+ve	-ve
8	2	M	+ve	+ve	+ve	+ve	+ve
9	1.2	F	+ve	+ve	-ve	+ve	-ve
10	13	M	+ve	-ve	+ve	+ve	+ve

Abn. indicates abnormalities; UL, upper limbs.

data were presented as mean and SD. There was no significant difference in MD and FA on both sides of patients and controls. Hence, the values obtained from both sides were combined. The mean and SD of the FA and MD of different regions of the brain in the patients and controls were calculated. Normally distributed data were compared between the 2 groups using independent-samples *t* test. Data that violated the normality assumptions were compared using the Mann-Whitney test. Probability (*P*) values less than 0.05 were considered statistically significant. The receiver operating characteristic (ROC) curve was done to evaluate the diagnostic capability of the FA and MD in differentiating patients from controls, with the calculation of the area under the curve (AUC), accuracy, sensitivity, and specificity.

**RESULTS**

Patients presented with extrapyramidal signs in the form of hyperreflexia (n = 8), tone abnormalities (n = 8), and neuromotor incoordination (n = 7). Other signs were decreased motor power of both the upper limbs (n = 7), and executive, cognitive, and motor

abnormalities (n = 6). Table 1 shows the demographic data of the patients.

On routine MRI, there was no area of abnormal signal intensity in the gray and white matter of patients and controls. Table 2 shows MD and FA of the gray matter regions of patients and controls. There was a significantly higher MD of the globus pallidus, thalamus, caudate head, substantia nigra, and dentate nucleus in patients than in controls (*P* = 0.007, 0.001, 0.014, 0.003, and 0.002), respectively. There was a nonsignificant difference in FA of all gray matter regions (Fig. 2). At ROC curve (Table 3), the AUCs of MD of the globus pallidus and thalamus used to differentiate patients from controls were 0.93 and 0.925, respectively. Selection of 0.77 and  $0.74 \times 10^{-3}$  mm<sup>2</sup>/s as a cutoff point of globus pallidus and thalamus revealed sensitivity values of 90% and 90%, specificity values of 80% 90%, and accuracy values of 75% and 90%, respectively (Fig. 3).

There was a significant higher MD of the frontal white matter and posterior limb of the internal capsule in patients compared with controls (*P* = 0.001 and 0.02), respectively. There were nonsignificant differences in MD of the parietal, temporal, and occipital regions (*P* = 0.82, 0.34, and 0.26), respectively (Table 4; Fig. 4). At ROC curve (Table 5), the AUCs of the MD of the frontal white matter and posterior limb of the internal capsule used to differentiate patients from controls were 0.82 and 0.80, respectively. Selection of 0.90 and  $0.78 \times 10^{-3}$  mm<sup>2</sup>/s as a cutoff point of MD of the frontal white matter and posterior limb of the internal capsule revealed sensitivity values of 90% and 80%, specificity values of 70% and 80%, and accuracy values of 80% and 80%, respectively (Fig. 5).

**TABLE 2.** The Mean and SD of MD and FA of the Selected Gray Matter Regions

Variable	Region	Patients (n = 10), Mean ± SD	Controls (n = 10), Mean ± SD	<i>P</i>
MD	Globus pallidus	0.83 ± 0.06	0.71 ± 0.10	0.007
	Thalamus	0.84 ± 0.08	0.67 ± 0.09	0.001
	Caudate head	0.89 ± 0.15	0.77 ± 0.02	0.014
	Substantia nigra	0.92 ± 0.11	0.79 ± 0.03	0.003
	Dentate nucleus	0.82 ± 0.04	0.71 ± 0.09	0.002
FA	Globus pallidus	0.30 ± 0.08	0.24 ± 0.05	0.09
	Thalamus	0.24 ± 0.07	0.26 ± 0.04	0.49
	Caudate head	0.16 ± 0.04	0.18 ± 0.04	0.32
	Substantia nigra	0.38 ± 0.11	0.39 ± 0.09	0.83
	Dentate nucleus	0.40 ± 0.06	0.39 ± 0.06	0.66

**TABLE 3.** Results of ROC Curve of MD of Gray Matter Used for Differentiating Patients From Controls

Variable	ROI Site	Cutoff Value	AUC	Sens., %	Spec., %	Accuracy, %
MD	Globus P	0.765	0.93	90	80	75
	Thalamus	0.735	0.925	90	90	90
	Caudate H	0.775	0.87	80	90	85
	Substantia N	0.825	0.77	70	70	70
	Dentate N	0.785	0.86	80	70	75

Caudate H indicates caudate head; Dentate N, dentate nucleus; Globus P, globus pallidus; Sens., sensitivity; Spec., specificity; Substantia N, substantia nigra.

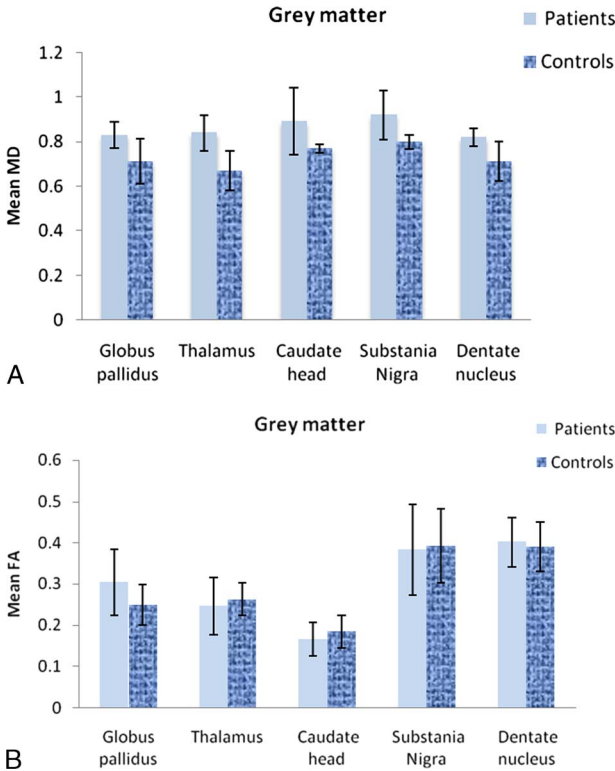


**FIGURE 2.** Bar graph of DTI parameters of gray matter regions. A, There is a significant higher MD of the globus pallidus ( $P = 0.007$ ), thalamus ( $P = 0.001$ ), caudate head ( $P = 0.014$ ), substantia nigra ( $P = 0.003$ ), and dentate nucleus ( $P = 0.002$ ) in patients than in controls. B, There is an insignificant FA value of the globus pallidus ( $P = 0.09$ ), thalamus ( $P = 0.49$ ), caudate head ( $P = 0.32$ ), substantia nigra ( $P = 0.83$ ), and dentate nucleus ( $P = 0.66$ ) in patients than in controls.

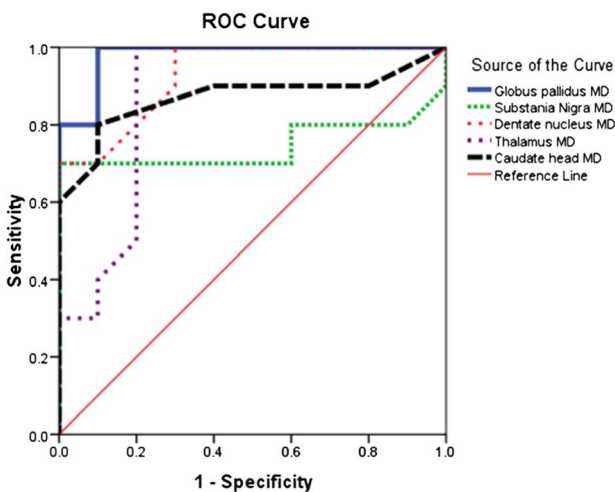


**FIGURE 3.** Receiver operating characteristic curve of MD gray matter regions: the AUCs of MD of the globus pallidus and thalamus used to differentiate patients from controls were 0.93 and 0.925, respectively. Selection of  $0.77$  and  $0.74 \times 10^{-3} \text{ mm}^2/\text{s}$  as a cutoff point of globus pallidus and thalamus revealed sensitivity values of 90% and 90%, specificity values of 80% and 90% and accuracy values of 75% and 90%, respectively.

**TABLE 4.** Mean, SD, Minimum, and Maximum of FA and MD of the Selected WM Regions

Variable	ROI Site	Patients (n = 10)	Controls (n = 10)	P
MD	Frontal WM	$1.12 \pm 0.21$	$0.82 \pm 0.04$	0.001
	PL internal C	$0.82 \pm 0.08$	$0.75 \pm 0.04$	0.02
	Parietal WM	$0.81 \pm 0.04$	$0.82 \pm 0.03$	0.46
	Temporal WM	$0.82 \pm 0.03$	$0.81 \pm 0.04$	0.45
	Occipital WM	$0.88 \pm 0.12$	$0.83 \pm 0.06$	0.26
FA	Frontal WM	$0.36 \pm 0.07$	$0.46 \pm 0.09$	0.006
	PL Internal C	$0.46 \pm 0.11$	$0.64 \pm 0.16$	0.006
	Parietal WM	$0.51 \pm 0.02$	$0.52 \pm 0.03$	0.82
	Temporal WM	$0.52 \pm 0.02$	$0.51 \pm 0.03$	0.34
	Occipital WM	$0.48 \pm 0.09$	$0.53 \pm 0.09$	0.25

C indicates capsule; PL, posterior limb; WM, white matter.

There was a significant lower FA ( $P = 0.006$  and  $0.006$ ) of the frontal lobe white matter and posterior limb of the internal capsule in patients compared with controls, respectively. There was a nonsignificant difference in FA and MD of the parietal, temporal, and occipital white matter of patients versus controls ( $P = 0.82$ ,  $0.34$ , and  $0.26$ ), respectively (Table 4; Fig. 4). At ROC curve (Table 5), the AUCs of the FA values of the frontal white matter and posterior limb of the internal capsule used to differentiate

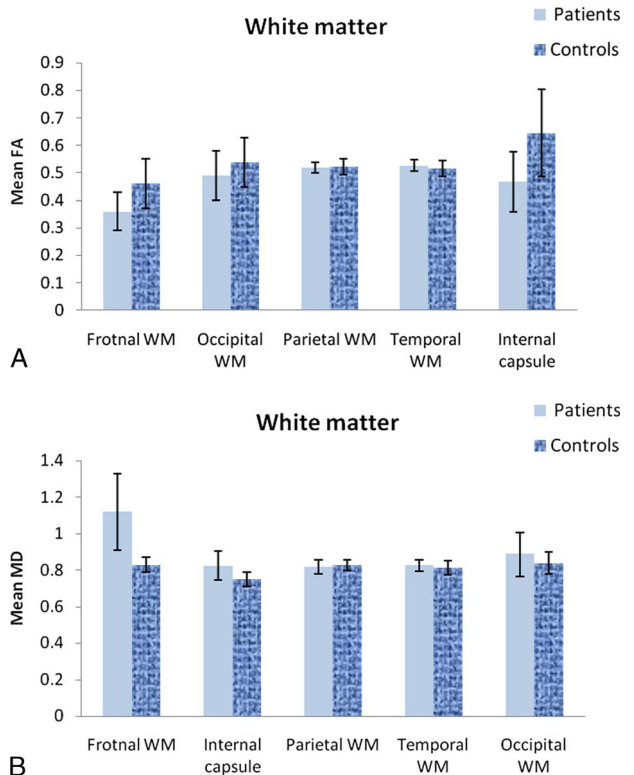


**FIGURE 4.** Bar graph of DTI parameters of white matter between patients and controls. A, There is a significant lower FA value of the frontal white matter ( $P = 0.006$ ) and posterior limb of the internal capsule ( $P = 0.006$ ) in patients than in controls. B, There is a significant higher MD value of the frontal white matter ( $P = 0.001$ ) and posterior limb of the internal capsule ( $P = 0.02$ ) in patients than in controls.

**TABLE 5.** Results of ROC Curve of FA and MD of WM in Differentiating Patients From Controls

Variable	ROI Site	Cutoff Value	Sens., AUC	Spec., %	Accuracy, %
FA	Frontal WM	0.38	0.83	70	80
	PL Internal C	0.52	0.85	90	75
MD	Frontal WM	0.9	0.81	90	80
	PL Internal C	0.775	0.80	80	80

C indicates capsule; PL, posterior limb; Sens., sensitivity; Spec., specificity; WM, white matter.

patients from controls were 0.83 and 0.85. Selection of 0.38 and 0.53 as a cutoff FA of the frontal lobe white matter and posterior limb of the internal capsule revealed sensitivity values of 70% and 90%, specificity values of 90% and 60%, and accuracy values of 80% and 75%, respectively (Fig. 5).

The high MD of the cerebellar dentate nucleus was associated with neuromuscular incoordination (n = 7), and high MD of the basal ganglia and substantia nigra was associated with muscle tone and reflexes abnormalities (n = 8). Abnormal high MD and low FA of the frontal white matter were associated with executive function abnormality (n = 6), and those of the posterior limb of the internal capsule were associated with decreased motor power of both the upper limbs (n = 7). There was a positive correlation between MD of the globus pallidus and the highest bilirubin level in patients (r = 0.87 and P = 0.001).

**DISCUSSION**

The main findings in this work are that there is a significantly higher MD of the gray matter regions in patients with Crigler-Najjar-syndrome type I than in controls. There is also significantly higher MD and lower FA of the frontal white matter and posterior limb of the internal capsule of patients, and the DTI parameters of the gray and white matter well correlated with neurological findings and the highest bilirubin level.

Conventional MRI can detect abnormal high signal intensity on T2-weighted images and FLAIR images of the ganglionic region or even deep gray matter caused by chronic hyperbilirubinemia.<sup>9-12</sup> In contrast, we did not find any signal abnormality (on T2-weighted

images or FLAIR images) in our patient group. This could be explained by the damage in the brain tissues, which was under the minimum level to be detected by conventional MRI.

In this study, DTI can detect changes in the gray and white matter that did not appear at routine MRI. This is explained by DTI parameters becoming abnormal before morphological changes at conventional MR owing to its sensitivity to microstructural changes of the brain parenchyma. The FA and MD may vary independently because the damaged brain tissue has glial and neuronal cells and changes of MD are related to mainly isotropic nature of the gray matter. Diffusion tensor imaging also improved sensitivity and objectivity in early detection of minor developmental and long-term changes along specific anatomical pathways that could be missed by the relatively subjective conventional MRI.<sup>17-20,31</sup>

In this study, there is statistically significant higher MD and nonsignificant FA of selected gray matter regions of patients, especially the globus pallidus and thalamus. The effect on isotropy reported in the selected gray matter regions is related to chronic exposure of brain parenchyma to high levels of unconjugated hyperbilirubinemia and consequently its cytotoxic effect resulting in cell death through increasing intracellular calcium, which leads to activation of proteolytic enzymes (proteases, lipases, and endonucleases), apoptosis, necrosis, and cell cycle arrest. When the cell death process is completed, the diffusion became unrestricted because of cell loss and an increase of the extracellular spaces with subsequently high MD values. There are nonsignificant changes in FA of gray matter regions because FA is sensitive to abnormalities of the anisotropic diffusion, which is present in the white matter, not in the gray matter.<sup>18-24</sup>

In this work, there is a statistical significant decrease in FA and an increase in MD of the frontal white matter and posterior limb of the internal capsule in the patient group. The decreased FA could be attributed to the anisotropic nature of diffusion of the white matter with sensitivity of FA to the low values of diffusion anisotropy, making FA providing useful information about pathological changes of the white matter. The effect on the anisotropy of the white matter could be attributed to the toxic effect of the unconjugated hyperbilirubinemia leading to cell death subsequent to demyelination, and because myelin is the most important factor in the presence of anisotropy, changes in the anisotropy and FA values appear. The high MD of the selected white matter regions could be explained also by the cell death with subsequent increased extracellular spaces leading to unrestricted diffusion.<sup>20-25</sup>

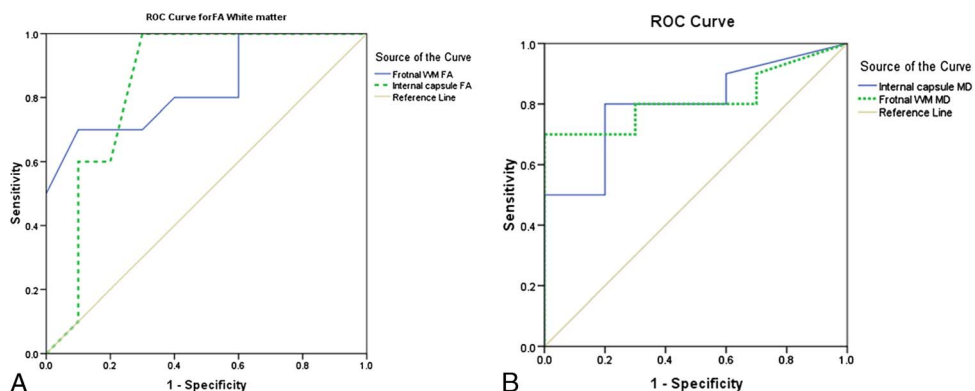


**FIGURE 5.** Receiver operating characteristic curve of white matter regions. A, The AUCs of the MD of the frontal white matter and posterior limb of the internal capsule used to differentiate patients from controls were 0.82 and 0.80, respectively. Selection of 0.90 and  $0.78 \times 10^{-3} \text{ mm}^2/\text{s}$  as a cutoff point of MD of the frontal white matter and posterior limb of internal capsule revealed sensitivity values of 90% and 80%, specificity values of 80% and 80%, and accuracy values of 80% and 80%, respectively. B, The AUCs of FA of the frontal white matter and posterior limb of the internal capsule used to differentiate patients from controls were 0.83 and 0.85. Selection of 0.38 and 0.53 as a cutoff FA of the frontal lobe white matter and posterior limb of the internal capsule revealed sensitivity values of 70% and 90%, specificity values of 90% and 60%, and accuracy values of 80% and 75%, respectively.

In this study, abnormalities in DTI parameter of the selected regions of the gray and white matter of the patients are correlated and coping with the clinical presentation and neurological findings of the patients. The changes in MD of the gray matter correlated with extrapyramidal signs of the patients in the form of neuromuscular incoordination, and abnormalities in the muscle tone and reflexes. In addition, the changes in MD and FA of the frontal white matter and posterior limb of the internal capsule correlated with an abnormality in the executive function and a decrease in the motor power of both the upper limbs of these patients.

In this study, there is a strong positive correlation of the MD of gray matter regions with the highest serum bilirubin level. This can be attributed to the cytotoxic effect of unconjugated bilirubin, which increases with the high level of bilirubin in the blood leading to more cell death and the associated destruction of the blood-brain barrier.

There are few limitations of this study. First, this study included a small number of patients. Further multicenter studies on a large number of patients will improve the results. Second, this study used DTI on a 1.5-T scanner using ROI. Further studies using multiparametric MRI of proton MR spectroscopy and arterial spin labeling using higher tesla scanners with the application of advanced postprocessing and machine learning<sup>18,32–35</sup> will improve the results. The third limitation is the absence of serial DTI follow-up of patients, so further studies with serial follow-up with DTI are recommended for better evaluation.

## CONCLUSIONS

Diffusion tensor imaging can detect microstructural changes of the deep gray matter and some regions of the white matter in children with Crigler-Najjar syndrome type I that could not be detected by conventional MRI. Changes occur not only in the deep gray matter but also in some areas of white matter.

## REFERENCES

- Ebrahimi A, Rahim F. Crigler-Najjar syndrome: current perspectives and the application of clinical genetics. *Endocr Metab Immune Disord Drug Targets*. 2018;18:201–211.
- Kumar P, Sasmal G, Gupta S, et al. Crigler Najjar syndrome type 2 (CNS type 2): an unwonted cause of jaundice in adults. *J Clin Diagn Res*. 2017;11:OD05–OD06.
- Maruo Y, Nakahara S, Yanagi T, et al. Genotype of UGT1A1 and phenotype correlation between Crigler-Najjar syndrome type II and Gilbert syndrome. *J Gastroenterol Hepatol*. 2016;31:403–408.
- Li L, Deng G, Tang Y, et al. Spectrum of UGT1A1 variations in Chinese patients with Crigler-Najjar syndrome type II. *PLoS One*. 2015;10:e0126263.
- van Dijk R, Beuers U, Bosma PJ. Gene replacement therapy for genetic hepatocellular jaundice. *Clin Rev Allergy Immunol*. 2015;48:243–253.
- Memon N, Weinberger BI, Hegyi T, et al. Inherited disorders of bilirubin clearance. *Pediatr Res*. 2016;79:378–386.
- Bhutani VK, Wong R. Bilirubin-induced neurologic dysfunction (BIND). *Semin Fetal Neonatal Med*. 2015;20:1.
- Bhutani VK, Johnson-Hamerman L. The clinical syndrome of bilirubin-induced neurologic dysfunction. *Semin Fetal Neonatal Med*. 2015;20:6–13.
- Ribeiro BN, Lima GA, Ventura N, et al. Chronic kernicterus: magnetic resonance imaging findings. *Radiol Bras*. 2016;49:407–408.
- van Toorn R, Brink P, Smith J, et al. Bilirubin-induced neurological dysfunction: a clinico-radiological-neurophysiological correlation in 30 consecutive children. *J Child Neurol*. 2016;31:1579–1583.
- Watchko JF. Bilirubin-induced neurotoxicity in the preterm neonate. *Clin Perinatol*. 2016;43:297–311.
- Wisnowski JL, Panigrahy A, Painter MJ, et al. Magnetic resonance imaging abnormalities in advanced acute bilirubin encephalopathy highlight dentato-thalamo-cortical pathways. *J Pediatr*. 2016;174:260–263.
- Rose J, Vassar R. Movement disorders due to bilirubin toxicity. *Semin Fetal Neonatal Med*. 2015;20:20–25.
- Wisnowski JL, Panigrahy A, Painter MJ, et al. Magnetic resonance imaging of bilirubin encephalopathy: current limitations and future promise. *Semin Perinatol*. 2014;38:422–428.
- Sarı S, Yavuz A, Batur A, et al. Brain magnetic resonance imaging and magnetic resonance spectroscopy findings of children with kernicterus. *Pol J Radiol*. 2015;80:72–80.
- Wang X, Wu W, Hou BL, et al. Studying neonatal bilirubin encephalopathy with conventional MRI, MRS, and DWI. *Neuroradiology*. 2008;50:885–893.
- Tae WS, Ham BJ, Pyun SB, et al. Current clinical applications of diffusion-tensor imaging in neurological disorders. *J Clin Neurol*. 2018;14:129–140.
- Abdel Razek AAK. Routine and advanced diffusion imaging modules of the salivary glands. *Neuroimaging Clin N Am*. 2018;28:245–254.
- El-Serougy L, Abdel Razek AA, Ezzat A, et al. Assessment of diffusion tensor imaging metrics in differentiating low-grade from high-grade gliomas. *Neuroradiol J*. 2016;29:400–407.
- Tamnes CK, Roalf DR, Goddings AL, et al. Diffusion MRI of white matter microstructure development in childhood and adolescence: methods, challenges and progress. *Dev Cogn Neurosci*. 2018;33:161–175.
- Khalek Abdel Razek AA. Characterization of salivary gland tumours with diffusion tensor imaging. *Dentomaxillofac Radiol*. 2018;47:20170343.
- Razek AAKA, Batouty N, Fathy W, et al. Diffusion tensor imaging of the optic disc in idiopathic intracranial hypertension. *Neuroradiology*. 2018;60:1159–1166.
- Agarwal N, Tekes A, Poretti A, et al. Pitfalls in diffusion-weighted and diffusion tensor imaging of the pediatric brain. *Neuropediatrics*. 2017;48:340–349.
- Ho ML, Campeau NG, Ngo TD, et al. Pediatric brain MRI, part 2: advanced techniques. *Pediatr Radiol*. 2017;47:544–555.
- Razek AA, Shabana AA, Elsaied TO, et al. Diffusion tensor imaging of mild-moderate carpal tunnel syndrome: correlation with nerve conduction study and clinical tests. *Clin Rheumatol*. 2017;36:2319–2324.
- Yan R, Han D, Ren J, et al. Diagnostic value of conventional MRI combined with DTI for neonatal hyperbilirubinemia. *Pediatr Neonatol*. 2018;59:161–167.
- Watchko JF, Painter MJ, Panigrahy A. Quantitative ADC in bilirubin encephalopathy. *Jpn J Radiol*. 2013;31:299–300.
- Cece H, Abuhandan M, Cakmak A, et al. Diffusion-weighted imaging of patients with neonatal bilirubin encephalopathy. *Jpn J Radiol*. 2013;31:179–185.
- Touwen BCL. *Examination of the Child With Minor Neurological Dysfunctions*. 2nd ed. *Clinics in Developmental Medicine, No. 71*. London: SIMP With Heinemann Medical. Philadelphia: Lippincott, Williams and Wilkins; 1979.
- Hadders-Algra M, Heineman KR, Bos AF, et al. The assessment of minor neurological dysfunction in infancy using the Touwen infant neurological examination: strengths and limitations. *Dev Med Child Neurol*. 2010;52:87–92.
- Jašprová J, Dal Ben M, Humý D, et al. Neuro-inflammatory effects of photodegradative products of bilirubin. *Sci Rep*. 2018;8:7444.
- Abdel Razek AAK. Arterial spin labelling and diffusion-weighted magnetic resonance imaging in differentiation of recurrent head and neck cancer from post-radiation changes. *J Laryngol Otol*. 2018;132:923–928.
- Razek AA, Nada N. Correlation of choline/creatine and apparent diffusion coefficient values with the prognostic parameters of head and neck squamous cell carcinoma. *NMR Biomed*. 2016;29:483–489.
- Razek AAKA, El-Serougy L, Abdelsalam M, et al. Differentiation of residual/recurrent gliomas from post-radiation necrosis with arterial spin labeling and diffusion tensor magnetic resonance imaging-derived metrics. *Neuroradiology*. 2018;60:169–177.
- Razek AAKA. Diffusion tensor imaging in differentiation of residual head and neck squamous cell carcinoma from post-radiation changes. *MagnReson Imaging*. 2018;54:84–89.